

**What You See Is Not What You Get – On the Accuracy of Voxel-Based Dosimetry in
Molecular Radiotherapy**

Authors:

Dr. Johannes Tran-Gia*

M.Sc. Maikol Salas-Ramirez

Prof. Dr. Michael Lassmann

Affiliation:

Department of Nuclear Medicine

University of Würzburg

Oberdürrbacher Str. 6

97080 Würzburg, Germany

***Corresponding Author**

Phone: +49-931-201-35421

Email: Tran_J@ukw.de

Running Title:

On the Accuracy of Voxel-Based Dosimetry

Word Count:

This manuscript contains > 5,000 words.

ABSTRACT

Due to improvements in quantitative SPECT/CT, voxel-based dosimetry for radionuclide therapies has aroused growing interest as it promises the visualization of absorbed doses at a voxel level. In this work, SPECT/CT-based voxel-based dosimetry of a 3D printed 2-compartment kidney phantom was performed, and the resulting absorbed dose distributions were examined. Additionally, the potential of the PETPVC partial-volume correction tool was investigated.

Methods

Both kidney compartments (70% cortex, 30% medulla) were filled with different activity concentrations and SPECT/CT imaging was performed. The images were reconstructed using varying reconstruction settings (iterations, subsets, and post-filtering). Based on these activity concentration maps, absorbed dose distributions were calculated with pre-calculated Lu-177 voxel S values and an empirical kidney half-life. An additional set of absorbed doses was calculated after applying PETPVC for partial-volume correction of the SPECT reconstructions.

Results

SPECT/CT imaging blurs the two discrete sub-organ absorbed dose values into a continuous distribution. While this effect is slightly improved by applying more iterations, it is enhanced by additional post-filtering. By applying PETPVC, the absorbed dose values are separated into 2 peaks. Although this leads to a better agreement between SPECT/CT-based and nominal values, considerable discrepancies remain. In contrast to the calculated nominal absorbed doses of 7.8/1.6 Gy (cortex/medulla), SPECT/CT-based voxel-level dosimetry resulted in mean absorbed doses ranging from 3.0-6.6 Gy (cortex) and 2.7-5.1 Gy (medulla). PETPVC led to improved ranges of 6.1-8.9 Gy (cortex) and 2.1-5.4 Gy (medulla).

Conclusion

Our study shows that Lu-177 quantitative SPECT/CT imaging leads to voxel-based dose distributions largely differing from the real organ distribution. SPECT/CT imaging and reconstruction deficiencies might directly translate into unrealistic absorbed dose distributions, thus questioning the reliability of SPECT-based voxel-level dosimetry. Therefore, SPECT/CT reconstructions should be adapted to ensure an accurate quantification of the underlying activity and, therefore, absorbed dose in a volume-of-interest of the expected object size (e.g. organs, organ sub-structures, lesions or voxels). As an example, PETPVC largely improves the match between SPECT/CT-based and nominal dose distributions.

In conclusion, the concept of voxel-based dosimetry should be treated with caution. Specifically, it should be kept in mind that the absorbed dose distribution is mainly a convolved version of the underlying SPECT reconstruction.

INTRODUCTION

Molecular radiotherapy (MRT) aims at delivering a lethal radiation dose to a pathological region (e.g. tumors). Personalized dosimetry would be desirable to maximize therapeutic efficacy by using patient-specific administered doses while avoiding toxicity to healthy organs (e.g. the kidney). In external beam radiotherapy, the relationship between dose and tumor response or organ toxicity is well understood and dosimetry has, therefore, been established in the clinical workflow. Due to the external ionizing radiation source, treatment simulation is performed e.g. based on Monte-Carlo simulations of the energy deposition by photons and electrons emitted from a well-controlled, nearly monoenergetic beam (*1*).

In contrast, the distribution of a radiopharmaceutical in a patient to be treated with MRT depends on the patient-specific metabolism. Therefore, MRT dosimetry based on quantitative imaging can only be performed after the administration of either a small pre-therapeutic quantity of the radiopharmaceutical or after a first or several treatment cycles. The patient scans typically lead to heterogeneous activity distributions either quantified with positron emission tomography (PET) or single photon emission computed tomography (SPECT) in combination with computed tomography (CT). As both techniques suffer from considerable degradations caused by noise and resolution limitations (resulting in the so-called partial-volume errors), absorbed organ dose distributions derived from these activity distributions suffer from the same insufficiencies, thus greatly limiting the accuracy of dosimetry in MRT treatments.

In external beam therapy, dose volume histograms (DVHs) present a valuable tool for treatment planning as well as calculation of tumor control probability and normal tissue complication probability (*2,3*). Although, over the past years, a wide range of tools for an improved determination of voxelized three-dimensional (3D) internal dose distributions has been

proposed (4-9), nuclear medicine imaging based dose volume histograms suffer from partial-volume errors and can only provide a rough estimate of the underlying radionuclide distribution. Even though partial-volume errors in SPECT/CT imaging can be effectively reduced by selecting an optimized combination of iteration number and post-reconstruction filtering, visible residual degradations always remain (2). Nevertheless, DVHs are a helpful tool to visualize and to quantify spatially inhomogeneous absorbed dose distributions.

A large number of different methods for compensating partial-volume errors have been proposed in the past (10). Most of these partial-volume corrections have been successfully applied and tested in PET/CT imaging (11-13). While the rather simplistic concept of volume-dependent, pre-determined recovery coefficients, which was initially introduced for PET/CT imaging, has been successfully adopted for SPECT/CT imaging (14-16), not many attempts have been made to adopt more sophisticated partial-volume correction methods for SPECT/CT quantification.

To fill this gap, the aim of this work was two-fold:

a) To analyze the influence of SPECT/CT image reconstruction on 3D dose distributions, visualized by dose volume histograms. In contrast to (2), where Monte Carlo simulated data was used to assess the quality of the image reconstruction, an inhomogeneous kidney activity distribution was obtained by imaging a 3D printed two-compartment kidney filled with different activity concentrations (17) on a clinical SPECT/CT system. Two reconstruction algorithms were investigated: the widely used ordered subset expectation maximization (here: Flash3D) and a recently proposed ordered subset conjugate gradient minimization (xSPECT Quant).

b) To reduce SPECT-inherent residual degradations remaining even for fine-tuned standard SPECT reconstructions by introducing a post-reconstruction partial-volume correction. Due to its

non-commercial nature and simple user interface, the PETPVC (18) partial-volume correction tool was chosen for that purpose.

METHODS

Filling of the 2-Compartment Kidney Phantom

In this study, a previously presented 3D printed 2-compartment kidney with a cortical compartment (70%) and a compartment containing medulla and collecting system (30%) was used to mimic a nonuniform kidney activity distribution. The modeling, printing, and refinement procedure, as well as the attachment system for the National Electrical Manufacturers Association (NEMA)-NU2-2012 body phantom (PTW-Freiburg), are described comprehensively in (17) and (19). A technical drawing of the phantom including the most relevant dimensions is given in Figure 1 (filling volume cortex: 99.6 mL, filling volume medulla: 44.0 mL). Nonuniform kidney uptake was achieved by filling both compartments with radioactive solutions of different activity concentrations. A ratio of 5:1 was chosen based on autoradiography data from de Jong et al. where, in the considered kidney regions, activity concentration ratios between 1:1 and 8:1 were found, depending on patient, time after injection, and sub-region of cortex or medulla (20). The ratio 5:1 1) marks the center of these observations, and 2) helps illustrating the difference between the two compartments and separate the absorbed dose peaks in the respective dose volume histograms. To ensure a stable solution, ^{177}Lu chloride (Isotope Technologies Garching GmbH) was dissolved in 0.1 M HCl with 100 ppm of stable lutetium for all measurements (21).

A VDC-405 activity meter with a VIK-202 ionization chamber (Comecer SpA) was used for estimating the activity concentration during the phantom filling process. Subsequently, accurate activity concentrations were obtained by measuring 1-mL aliquots of both stock solutions (3 per stock solution) in a high-purity germanium detector (HPGe; Canberra Industries

Inc.) whose energy-dependent efficiency was calibrated with several NIST (National Institute of Standards and Technology)– and NPL (National Physical Laboratory)–traceable standards over the energy range considered.

The amount of stock solution in each kidney compartment was determined by weighing the phantom before and after the filling procedure with a PCB 3500-2 precision balance (Kern & Sohn GmbH) with a readability of 0.01 g. In contrast, the aliquot volumes were weighed in an ED224S analytical balance (Sartorius AG) with a readability of 0.1 mg. All activities were decay-corrected to the starting time of the SPECT/CT acquisition.

Quantitative SPECT/CT imaging

All acquisitions were performed with a Symbia Intevo Bold SPECT/CT system (Siemens Healthineers) with 9.5-mm crystal thickness, medium-energy low-penetration collimator, 180° configuration, auto-contouring, continuous mode, 60 views, 30s per view, 256 × 256 matrix, and 3 energy windows (20% around the main photopeak of 208keV with 2 adjacent 10% windows). Subsequent to the SPECT acquisition, a low-dose CT was acquired for attenuation correction (130 kVp, 512×512×131 matrix, 1.0 × 1.0 × 3.0 mm³ resolution). Additionally, a low-dose CT with 1-mm isotropic resolution (130 kVp, 512×512×131 matrix) was acquired for a better volume of interest (VOI) definition.

Two different reconstruction algorithms were applied for each acquisition. The first, Flash3D, is ordered-subset expectation maximization with depth-dependent 3D resolution recovery (Gaussian point spread function model). Reconstructions were performed with a matrix of 128 as recommended by the manufacturer (voxel size, 4.8 mm). For quantitative imaging, an image calibration factor (ICF) of 20.22±0.53 cps/MBq (counts-per-second-per-Megabecquerel)

had been previously determined in a cylindrical Jaszczak phantom (22) (although an uncertainty for ICF was determined including the uncertainties of acquisition duration [1 second] and number of counts [square root of counts], it is dominated by the uncertainty of the HPGe-based activity determination, which was assumed as 2.5%). Based on this ICF, counts were converted to activity (MBq) by applying

$$Activity = \frac{\#Counts}{ICF \cdot Acquisition\ Duration}$$

The second type of reconstruction, xSPECT Quant, is ordered subset conjugate gradient maximization with depth-dependent 3D resolution recovery using a measured point spread function. As recommended by the manufacturer, a 256 matrix was used for the reconstruction (voxel size, 2.0 mm). For count–activity conversion, a manufacturer-determined class standard sensitivity (radionuclide-, collimator-, and crystal-dependent) is system specifically fine-tuned on the basis of a 3% NIST-traceable ⁷⁵Se source. For simplicity, xSPECT Quant will also be called xSPECT.

CT-based attenuation correction (in forward and backprojector) and a triple energy window scatter correction (in forward projector only) are applied in both reconstructions. To investigate the influence of the reconstruction parameters on the dose distribution, different combinations of updates (Flash3D: between 12 and 384 / xSPECT: between 12 and 96) and Gaussian post-filters (between 0 and 8 voxels) were applied. As the number of iterations is limited to 100 by the manufacturer, update numbers larger than 100 were obtained for Flash3D by applying a combination of iterations and subsets (e.g., 384 updates were obtained by combining 96 iterations with 4 subsets). While the combination of iterations and subsets has no impact on Flash3D reconstructions, this is not the case for xSPECT (22). Therefore, xSPECT was restricted to 1 subset.

All postprocessing was performed in MATLAB (MathWorks) and in syngo.via, version VB10B (Siemens Healthineers).

Partial-Volume Correction

First, VOIs were drawn in 3D Slicer (23) for both the cortex ($\text{VOI}_{\text{cortex}}$) as well as the medulla compartment ($\text{VOI}_{\text{medulla}}$) based on the isotropic-resolution CT (\rightarrow localization) in combination with the filling volumes (\rightarrow size). Next, the SPECT reconstructions (voxel sizes, 4.8/2.0 mm [Flash3D/xSPECT]) were interpolated to match the isotropic CT resolution of 1 mm (3D Slicer: bspline interpolation). Finally, partial-volume correction was performed using PETPVC (18) with iterative Yang (inputs: 1-mm SPECT interpolation, $\text{VOI}_{\text{cortex}}$, $\text{VOI}_{\text{medulla}}$, predetermined resolutions). This method was first presented in (10) and is an updated version of the region-based voxel-wise correction for PET (24). In short, it convolves the VOIs with the system's point spread function and uses the ratio before and after convolution to estimate partial-volume correction factors. Therefore, it corrects for spill-in and spill-out from one segmented VOI to another, but not from one voxel to another.

The necessary resolution estimates for all reconstruction parameter sets (Table 1) had previously been obtained in a matched-filter analysis of a hot-sphere–cold-background acquisition (six ^{177}Lu -filled spheres in the water-filled NEMA-NU2-2012 body phantom) reconstructed with the same reconstruction parameters as the SPECT image to be PVC-corrected. Both the image acquisition and the evaluation are described in detail in (22).

Calculation of Absorbed Dose Distributions

Dose distributions were obtained by convolution of the 1-mm isotropic SPECT interpolations (unit: MBq mL⁻¹) with a set of Monte-Carlo based voxel S values for ¹⁷⁷Lu (unit: mGy/MBq/s) as described in (25-27). Multiplication with the voxel volume (in milliliters) and a time-integrated activity coefficient of 73.6 h (estimated from a tissue-specific kidney half-life of 51 h (28) divided by ln(2)) yields the dose (mGy) in each voxel. This was performed for the uncorrected (no PVC) as well as the partial-volume corrected SPECT reconstructions (PETPVC).

Additionally, ground truth dose distributions were calculated by performing the above calculations on a numerical phantom consisting of VOI-based masks (0: non-active field-of-view, 1: active volume) multiplied with the HPGe-based activity concentration of the respective compartment.

Dose Volume Histograms

In the Results section, dose distributions will mainly be depicted as dose volume histograms (3). After discarding all voxels outside both sub-organ VOIs, differential DVHs assign all voxels in a certain absorbed dose interval to appropriate histogram bins (width: 25 mGy), which are normalized to the total number of voxels. As a continuation, cumulative DVHs are calculated as one minus the integral of the differential DVHs. While the horizontal axis represents the absorbed dose threshold for each bin, the vertical axis represents the fraction of the VOI volume having a dose larger than or equal to the dose threshold.

Calculation of Mean Sub-Organ Absorbed Doses

Mean sub-organ absorbed doses were calculated as mean over the CT-based sub-organ VOIs (VOI_{cortex} , $VOI_{medulla}$). This calculation was additionally performed for the ground truth absorbed dose distributions, and percentage differences were calculated.

As alternative measure to the mean absorbed dose, the root-mean-square deviation RMSD (square root of the mean squared voxel-wise difference) between the SPECT/CT-based and the nominal absorbed dose distribution was calculated as

$$RMSD = \sqrt{\frac{\sum_i [D_{SPECT/CT}(i) - D_{Nominal}(i)]^2}{\#Voxels}}.$$

Here, $D(i)$ stands for the absorbed dose in voxel i and the sum is taken over all voxels of the VOI.

RESULTS

As 3D-OSEM (ordered subset expectation maximization) with CT-based attenuation correction, triple energy window scatter correction and resolution recovery is the current gold standard in SPECT/CT imaging, only the Flash3D results will be given in the manuscript for reasons of clarity. The data for the very recently introduced and not yet widespread xSPECT Quant reconstruction will be shown as supplemental material in the appendix.

Activity Concentration versus Absorbed Dose Distribution

The kidney compartments were filled with activity concentrations of 1.89 ± 0.05 MBq/mL (cortex) and 0.36 ± 0.01 MBq/mL (medulla), representing a cortex-to-medulla-ratio of 5.21 ± 0.18 (based on HPGe measurements; an uncertainty of 1 mg was assumed for the aliquot volume – filled minus empty measurement vial– in addition to the 2.5% uncertainty of the HPGe-based activity determination). The CT-based VOI analysis resulted in sub-organ absorbed dose values of 7.75 Gy (cortex) and 1.56 Gy (medulla).

Figure 2 shows example distributions of activity concentration (MBq/mL) and the resulting absorbed dose distributions (Gy) before and after PVC. To visualize the differences, cross sections are additionally depicted. Despite slight smoothing especially at the sharp edges (e.g. around the transition between cortex and medulla at ± 40 mm), the absorbed dose distribution visually closely resembles the activity distribution. In consequence, the absorbed dose distribution is mainly influenced by the SPECT image reconstruction method and the related artifacts and errors. PETPVC effectively reduces partial-volume errors by shifting the counts back into the two VOIs.

Visual Assessment of Absorbed Dose Distributions

Figure 3 shows differential DVHs. For the sake of clarity, only a few example iteration numbers are depicted. The gamma camera based SPECT imaging process blurs the two discrete absorbed dose values of both compartments (blue and red solid lines) into one continuous distribution. As a result, voxel absorbed doses mainly lie between the low medullary and the high cortical nominal sub-organ absorbed doses. This is especially pronounced before convergence is reached (e.g. after 12 updates). As more updates are applied, the distribution more and more broadens until it eventually extends into both nominal absorbed dose values (e.g. after 96 updates). Post-filtering reintroduces the blurring into the images and spreads the signal across the field-of-view, resulting in a shift of the higher absorbed voxel doses towards smaller values. The consequent DVHs look similar to the ones before convergence. This is also illustrated in

Figure 4 showing the effect of the different reconstruction parameters on the 3D dose distributions (voxel size: 1 mm): As expected, SPECT reconstructions are blurred versions of the underlying two-compartment object (Figure 4, right). While this effect is improved by applying more updates, it is even further enhanced by post-filtering (e.g. 12 updates without filtering closely resemble 96 updates with an 8-mm filter applied).

The situation changes after the application of PETPVC: While a large difference remains visible between the nominal and the SPECT/CT-based differential dose volume histograms (especially for small iteration numbers), two separate peaks start to become visible after a sufficient number of updates (e.g. 96 updates). While the peaks of the cortical absorbed dose

distributions increase with increasing iteration numbers, the ones of the medulla simultaneously decrease. The optimum for the cortex is reached after ~96 updates, whereas the medulla compartment optimum is not reached before ~400 updates (depending on the post-filter applied). In contrast to the non-PVC-corrected reconstructions, post-filtering improves the resolution of the two peaks (decrease in width). As a consequence, the best visual correlation is achieved by a sufficient iteration number combined with a post-filter of adequately large FWHM (e.g. 384 updates and a 2-voxel FWHM post-filter). This impression is reinforced by the associated images (Figure 4), where both VOIs consist of absorbed dose values in very similar ranges if 96 updates and a 4-voxel FWHM post-filter are applied in combination with PETPVC.

Lastly, cumulative DVHs are depicted in Figure 5. According to this illustration, the high absorbed doses (i.e. the cortex) are largely underestimated without PVC (even more after post-filtering). Although more updates slightly improve these errors, no reliable statement about the absorbed dose values can be made based on the cumulative DVHs. After PETPVC, high absorbed doses are largely overestimated if too many updates are applied without filtering. In agreement with the differential DVH observations, this effect is effectively improved by the post-filtering.

Mean Sub-Organ Absorbed Doses

Table 2 lists the nominal and the SPECT/CT-based sub-organ absorbed doses of cortex and medulla for different reconstructions (different update numbers, different post-filters, with/without PETPVC). While the nominal absorbed doses were 7.8/1.6 Gy (cortex/medulla), SPECT/CT imaging resulted in mean absorbed doses ranging from 3.0-6.6 Gy (cortex) and 2.7-5.1 Gy (medulla). PETPVC led to improved ranges of 6.1-8.9 Gy (cortex) and 2.1-5.4 Gy

(medulla). For a better visualization, Figure 6 depicts the percentage differences. For the cortex, the best correlation between measured and nominal distribution is reached for a sufficient number of updates combined with an adequate post-filter (96 updates and a 2-voxel post-filter) with PETPVC applied. For the medulla, the difference continues to decline even after the maximum number of updates applied (difference of 33.6% after 384 updates without post-filtering with PETPVC applied).

Although the ideal combination of number of updates and post-filtering slightly differs for the RMSD (96 updates and a 2-voxel post-filter, Table 3), a similar behavior can be seen.

xSPECT Quant

Most observations made for the OSEM-based Flash3D reconstruction also apply for the OSCGM-based xSPECT Quant reconstruction. To illustrate this, Supplemental Figures 1 to 4 are provided in analogy to the Flash3D figures given in the main manuscript.

DISCUSSION

All investigations were performed based on a SPECT/CT dataset of a kidney with inhomogeneous activity concentration, which was achieved by filling two separate compartments of a 3D printed kidney phantom with different activity concentrations. Although these two distinct dose values are a gross simplification compared to the activity distribution in a real patient kidney, the simplicity of this model facilitates a comprehensive investigation of the influence of different reconstruction parameters and a subsequent partial-volume correction on the derived (differential as well as cumulative) dose volume histograms. It should be mentioned that, in contrast to external beam radiotherapy where DVHs are typically calculated based on morphological imaging (e.g. CT) and eventually used for treatment planning, the concept is used in this work only to visualize and better understand the effect of imaging errors on absorbed dose distributions. Although voxel-based dosimetry holds a large potential for more sophisticated treatment planning such as the calculation of biologically effective doses or equivalent uniform doses (29), more basic research on the underlying imaging effects is needed for a solid understanding of opportunities and pitfalls.

According to (30), any SPECT/CT-based activity distribution or volume-of-interest (VOI) features a spread of absorbed dose values that can be caused by:

- a) Real activity heterogeneities.
- b) Energy deposition from particles emitted outside the organ.
- c) Partial-volume errors caused by the limited spatial resolution of the imaging system (spill-in / spill-out).
- d) Noise in the data collection.

As the aim of this study was to understand and optimize the effect of partial-volume errors on the dose distribution, the influence of a), b) and d) had to be minimized. The activity heterogeneity a) was precisely defined by filling the two-compartment phantom with two different, HPGe-measured activity concentrations. In addition, b) can be neglected for Lu-177 with its short electron range (several millimeters) and d) was kept to a minimum by collecting sufficient counts ($2 \cdot 10^6$ in the main energy window). That way, all other major confounding factors of the absorbed dose spread are minimized in the study setup, and the study is ideally suited for investigating the influence of errors caused by the partial-volume effect. Lastly, resolution modeling, which both applied reconstructions comprise, can impair image quality in addition to the above reasons. For the reconstructions performed in this work, no edge ringing artifacts were visible. As the dimensions of the investigated object (e.g. the cortex diameter) lie in the range of the spatial resolution, overshoots are a more likely consequence of the applied resolution modeling, which explains the occurrence of high absorbed voxel doses for the unfiltered reconstruction (e.g. after 960 Flash3D updates). However, no profound analysis of resolution model related errors was performed in this study.

Despite the unnaturally abrupt transition between low and high activity concentration in the investigated phantom, an optimized combination of reconstruction parameters (updates and post-filtering) with PETPVC led to considerably improved differential and cumulative DVHs. Consequently, the residual degradations observed in (2) can be even further reduced by introducing a partial-volume correction performed subsequent to a standard manufacturer reconstruction.

As the iterative Yang partial-volume correction method convolves the segmented VOIs with the system's point spread function, one major source of error lies in the resolution: While

PETPVC was developed for PET imaging with a nearly isotropic and spatially invariant resolution, SPECT imaging features an anisotropic and spatially variant resolution (22). Although resolution recovery –which is provided by most manufacturers– partly corrects these spatial resolution variations, the resolution remains to a large extent dependent on the distance between the detector and the imaged object or, in other words, on the position of the object in the SPECT field-of-view. To minimize the related error, the same phantom and, therefore, detector auto-contour was applied for both the resolution determination measurement and the kidney measurement. Moreover, both the sphere inserts and the kidney were measured in the center of rotation. Due to the small kidney dimensions of 4 cm × 12 cm × 6 cm and presuming a slow spatial variation of the resolution, the assumption of an isotropic and spatially invariant resolution seems acceptable. Nevertheless, a spatially variant partial-volume correction method would be preferable and should be developed and applied in future studies. In addition to the spatial variance of the resolution, the determination of the resolution represents a potential source of error, which is discussed in detail in (22,31).

Additionally, it should be kept in mind that iterative Yang partial-volume correction corrects for spill-in and spill-out between segmented VOIs instead of a voxel-by-voxel correction, which introduces a correlation between the voxels within each VOI. Despite this disadvantage, the method was chosen as it produces a voxel-by-voxel correction of the whole image, does not require any prior information about the activity distribution, and can be used with any number of VOIs.

Another source of error is the calculation of absorbed doses based on pre-simulated Lu-177 voxel S values. The very low emission probability (~11%) of the 208 keV gamma transition results in a negligible photon proportion of the absorbed dose. Likewise, the beta radiation of Lu-

177 only has a range of several millimeters in soft tissue, leading to almost the entire dose being deposited directly at the origin of the disintegration. This assumption is confirmed by the observation that the absorbed dose distribution corresponds, in good approximation, to a multiplication of the activity distribution with a constant dose conversion factor. Lastly, the kidney phantom as well as the body phantom were filled with aqueous solutions, justifying that the voxel S values had been simulated for soft tissue. Still, it has to be stated that full Monte Carlo simulations should be used when different tissue densities (other than soft tissue) or inter-voxel heterogeneities are deemed relevant (32).

The conjugate gradient based xSPECT reconstruction (data provided as Supplemental Figures 1 to 5) shows a 3-4 times faster convergence than the expectation maximization based Flash3D reconstruction. Therefore, 12 xSPECT iterations are approximately comparable to 36 to 48 Flash3D iterations (22). Additionally, xSPECT has a tendency to favor areas of high signal while suppressing areas of low signal. If too many iterations are applied, the signal in low-intensity voxels starts to drop to zero as counts are shifted towards the higher-intensity cortical region. This leads to the occurrence of zeros in the entire medulla region after 96 unfiltered xSPECT iterations (Supplemental Figure 5). Although the xSPECT-based determination of mean absorbed doses for the medulla compartment seem to be nearly perfect after 36-60 xSPECT updates, followed by post-filtering and after PETPVC (dashed lines in Supplemental Figure 4B), the entire medulla activity stems from the cortex from which activity is spilled back into the medulla by PETPVC rather than by intensity originally located in the medulla. Therefore, care should be taken to examine the fundamentals of each reconstruction carefully rather than simply transferring reconstruction parameters between the two different reconstruction methods.

Instead, for the investigated count and noise conditions, the number of xSPECT iterations should be limited to 48.

One important finding of this work is that –without partial-volume correction– none of the presently available reconstruction methods was able to achieve a cumulative dose volume histogram that would be acceptable for treatment planning as:

- a) The lower absorbed doses of the medullary compartment are considerably overestimated.
- b) The higher absorbed doses of the cortical compartment are considerably underestimated.

In addition, this study setup neglects any errors in the time-activity curve integration, as it is offered (either organ-based or voxel-based) by some software solutions. These errors include e.g. inaccurate image registration, inter- and intra-observer variability in the VOI drawing, as well as differences in the choice of an appropriate fit function. As the voxel-level information, despite excluding these sources of error, strongly differs from the “true” distribution, it seems more adequate to assess the absorbed dose on an organ level or, in case of large organs such as the liver, to divide the VOI into sub-VOIs consisting of multiple voxels each to minimize the systematic partial-volume based error.

Although a voxel-based dosimetry approach results in an absorbed dose value for each voxel, the distribution of these doses can strongly differ from the truth. Instead, it is strongly dependent on the SPECT reconstruction settings including but not limited to the applied number of updates and the post-filter.

CONCLUSION

Although voxel-based dosimetry promises information about the dose absorbed in any organ-at-risk on a sub-organ or even voxel level, the resulting dose distributions were, in our simple set-up of a 2-compartment kidney phantom containing activity in a 5:1 ratio (cortex:medulla), found to be strongly affected by the SPECT reconstruction algorithm and the chosen reconstruction parameters such as iterations, subsets, and Gaussian post-filtering. For most short-range theranostic beta emitters such as ^{177}Lu , the dose is mostly deposited directly at the origin of the disintegration. Consequently, SPECT/CT imaging and reconstruction deficiencies might directly translate into unrealistic absorbed dose distributions, thus questioning the reliability of SPECT/CT-based voxel-based dosimetry. Instead, the SPECT/CT reconstructions should be adequately corrected (e.g. by partial-volume corrections) to ensure an accurate quantification of the underlying activity and, therefore, absorbed dose, in a volume-of-interest of the expected object size (e.g. organs, organ sub-structures, lesions or voxels).

DISCLOSURE

No potential conflicts of interest relevant to this article exist.

FUNDING

This work was partly supported by the European Metrology Programme for Innovation and Research (EMPIR) project 15HLT06 MRTDosimetry (<http://mrtdosimetry-empir.eu/>). The EMPIR is jointly funded by the EMPIR participating countries within EURAMET and the European Union.

KEY POINTS

Question: Does the SPECT/CT-based distribution of absorbed doses coincide with the underlying dose distribution and can the quality of voxel-based absorbed dose distributions be improved by performing a partial volume correction?

Pertinent Findings: In a Lu-177 phantom study with an inhomogeneously filled 3D-printed two-compartment kidney (cortex & medulla), imaging-based dose volume histograms considerably differed from the underlying absorbed doses. Although the agreement was improved by partial volume correction, differences remain and therapy planning based on the resulting dose volume histograms should be treated with caution.

Implication for Patient Care: The quantification of SPECT/CT images should be adapted to adequately match the volume-of-interest size of organs, organ sub-structures, lesions or voxels and the sampling of time-activity curves for calculating absorbed doses.

REFERENCES

1. Chetty IJ, Curran B, Cygler JE, et al. Report of the AAPM Task Group No. 105: Issues associated with clinical implementation of Monte Carlo-based photon and electron external beam treatment planning. *Med Phys*. 2007;34:4818-4853.
2. Cheng L, Hobbs RF, Segars PW, Sgouros G, Frey EC. Improved dose-volume histogram estimates for radiopharmaceutical therapy by optimizing quantitative SPECT reconstruction parameters. *Phys Med Biol*. 2013;58:3631.
3. Drzymala R, Mohan R, Brewster L, et al. Dose-volume histograms. *Int J Radiat Oncol*. 1991;21:71-78.
4. Besemer AE, Yang YM, Grudzinski JJ, Hall LT, Bednarz BP. Development and validation of RAPID: A patient-specific Monte Carlo three-dimensional internal dosimetry platform. *Cancer Biother Radiopharm*. 2018;33:155-165.
5. Hippeläinen E, Tenhunen M, Sohlberg A. Fast voxel-level dosimetry for ^{177}Lu labelled peptide treatments. *Phys Med Biol*. 2015;60:6685.
6. Jackson PA, Beauregard JM, Hofman MS, Kron T, Hogg A, Hicks RJ. An automated voxelized dosimetry tool for radionuclide therapy based on serial quantitative SPECT/CT imaging. *Med Phys*. 2013;40:112503.
7. Kairemo K, Kangasmäki A. 4D SPECT/CT acquisition for 3D dose calculation and dose planning in ^{177}Lu -peptide receptor radionuclide therapy: Applications for clinical routine. In: Baum RP, Rösch F, eds. *Theranostics, Gallium-68, and Other Radionuclides*. Berlin Heidelberg: Springer; 2013:537-550.
8. Kost SD, Dewaraja YK, Abramson RG, Stabin MG. VIDA: a voxel-based dosimetry method for targeted radionuclide therapy using Geant4. *Cancer Biother Radio*. 2015;30:16-26.
9. Lee MS, Kim JH, Paeng JC, et al. Whole-body voxel-based personalized dosimetry: The multiple voxel S-value approach for heterogeneous media with nonuniform activity distributions. *J Nucl Med*. 2018;59:1133-1139.
10. Erlandsson K, Buvat I, Pretorius PH, Thomas BA, Hutton BF. A review of partial volume correction techniques for emission tomography and their applications in neurology, cardiology and oncology. *Phys Med Biol*. 2012;57:R119-159.
11. Rousset OG, Ma Y, Evans AC. Correction for partial volume effects in PET: Principle and validation. *J Nucl Med*. 1998;39:904-911.
12. Teo BK, Seo Y, Bacharach SL, et al. Partial-volume correction in PET: validation of an iterative postreconstruction method with phantom and patient data. *J Nucl Med*. 2007;48:802-810.

13. Tohka J, Reilhac A. Deconvolution-based partial volume correction in raclopride-PET and Monte Carlo comparison to MR-based method. *Neuroimage*. 2008;39:1570-1584.
14. Hoffman EJ, Huang SC, Phelps ME. Quantitation in positron emission computed tomography: 1. Effect of object size. *J Comput Assist Tomogr*. 1979;3:299-308.
15. Willowson K, Bailey DL, Baldock C. Quantitative SPECT reconstruction using CT-derived corrections. *Phys Med Biol*. 2008;53:3099-3112.
16. Srinivas SM, Dhurairaj T, Basu S, Bural G, Surti S, Alavi A. A recovery coefficient method for partial volume correction of PET images. *Ann Nucl Med*. 2009;23:341-348.
17. Tran-Gia J, Lassmann M. Optimizing image quantification for ^{177}Lu SPECT/CT based on a 3D printed 2-compartment kidney phantom. *J Nucl Med*. 2018;59:616-624.
18. Thomas BA, Cuplov V, Bousse A, et al. PETPVC: a toolbox for performing partial volume correction techniques in positron emission tomography. *Phys Med Biol*. 2016;61:7975.
19. Tran-Gia J, Schlögl S, Lassmann M. Design and fabrication of kidney phantoms for internal radiation dosimetry using 3D printing technology. *J Nucl Med*. 2016;57:1998-2005.
20. De Jong M, Valkema R, Van Gameren A, et al. Inhomogeneous localization of radioactivity in the human kidney after injection of [^{111}In -DTPA]octreotide. *J Nucl Med*. 2004;45:1168-1171.
21. Park MA, Mahmood A, Zimmerman RE, Limpa-Amara N, Makrigiorgos GM, Moore SC. Adsorption of metallic radionuclides on plastic phantom walls. *Med Phys*. 2008;35:1606-1610.
22. Tran-Gia J, Lassmann M. Characterization of noise and resolution for quantitative ^{177}Lu SPECT/CT with xSPECT Quant. *J Nucl Med*. 2019;60:50-59.
23. Fedorov A, Beichel R, Kalpathy-Cramer J, et al. 3D Slicer as an image computing platform for the quantitative imaging network. *Magn Reson Imaging*. 2012;30:1323-1341.
24. Thomas BA, Erlandsson K, Modat M, et al. The importance of appropriate partial volume correction for PET quantification in Alzheimer's disease. *Eur J Nucl Med Mol I*. 2011;38:1104-1119.
25. Kletting P, Schimmel S, Hänscheid H, et al. The NUKDOS software for treatment planning in molecular radiotherapy. *Z Med Phys*. 2015;25:264-274.
26. Fernández M, Hänscheid H, Mauxion T, et al. A fast method for rescaling voxel S values for arbitrary voxel sizes in targeted radionuclide therapy from a single Monte Carlo calculation. *Med Phys*. 2013;40:082502.

27. Pacilio M, Amato E, Lanconelli N, et al. Differences in 3D dose distributions due to calculation method of voxel S-values and the influence of image blurring in SPECT. *Phys Med Biol.* 2015;60:1945-1964.
28. Hänscheid H, Lapa C, Buck AK, Lassmann M, Werner RA. Dose mapping after endoradiotherapy with ¹⁷⁷Lu-DOTATATE/DOTATOC by a single measurement after 4 days. *J Nucl Med.* 2018;59:75-81.
29. Sgouros G, Frey E, Wahl R, He B, Prideaux A, Hobbs R. Three-dimensional imaging-based radiobiological dosimetry. *Semin Nucl Med.* 2008;38:321-334.
30. Ljungberg M, Frey E, Sjogreen K, Liu X, Dewaraja Y, Strand SE. 3D absorbed dose calculations based on SPECT: Evaluation for 111-In/90-Y therapy using Monte Carlo simulations. *Cancer Biother Radiopharm.* 2003;18:99-107.
31. Badger D, Barnden L. Spatial resolution is dependent on image content for SPECT with iterative reconstruction incorporating distance dependent resolution (DDR) correction. *Australas Phys Eng Sci Med.* 2014;37:551-557.
32. Bolch WE, Bouchet LG, Robertson JS, et al. MIRD pamphlet no. 17: The dosimetry of nonuniform activity distributions—radionuclide S values at the voxel level. *J Nucl Med.* 1999;40:11S-36S.

FIGURE 1

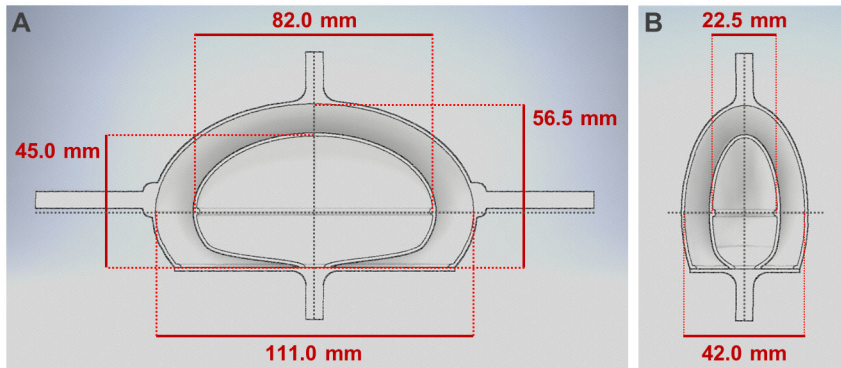


Figure 1. Technical drawing of the kidney phantom consisting of cortex and medulla. A and B represent perpendicular cross-sections.

FIGURE 2

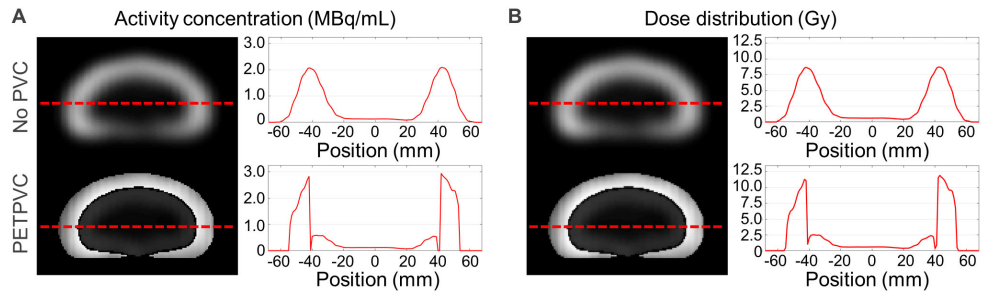


Figure 2. Difference between A: activity concentration (MBq/mL) and B: dose distribution (Gy). Shown are example images as well as cross sections (indicated by the dashed lines) before and after partial-volume correction (Flash3D with 48 iterations, 1 subset, and 8 mm Gaussian post-filter).

FIGURE 3

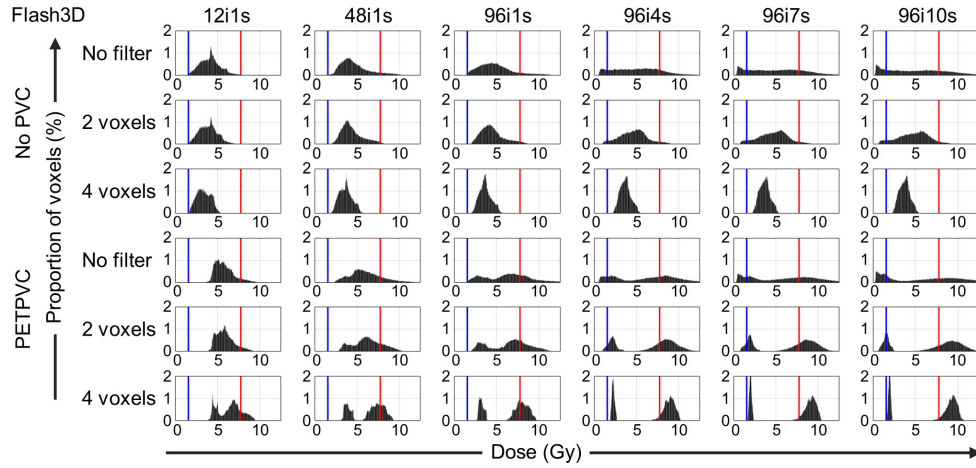


Figure 3. Differential dose volume histograms for different Flash3D reconstructions without (top) and with (bottom) partial-volume correction. From left to right, different numbers of updates (between 12 and 960) are shown. Additionally, different post-filters were applied (no filtering, 2-voxel FWHM, 4-voxel FWHM). The blue and red solid lines indicate the nominal absorbed dose values of both compartments.

FIGURE 4

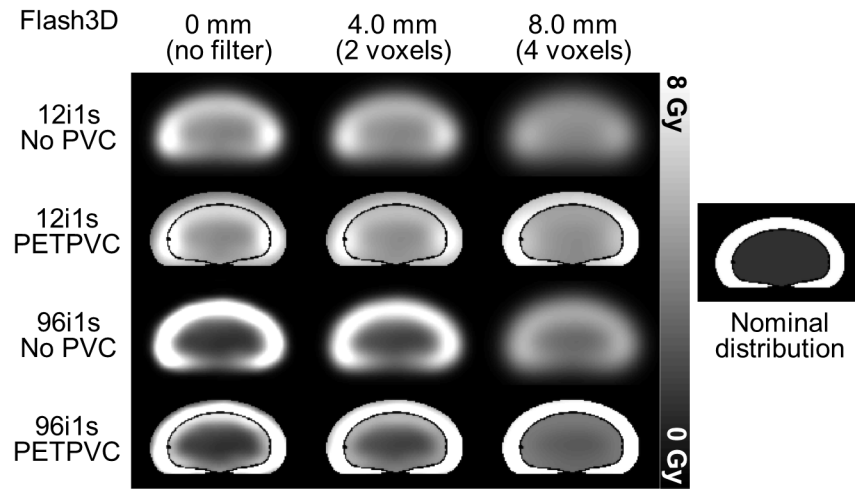


Figure 4. Cross-sections through the 3D absorbed dose distributions obtained from the Flash3D reconstructions (12 and 96 updates) with and without partial-volume correction. From left to right, different post-filters were applied (no filtering, 2-voxel FWHM, 4-voxel FWHM). Additionally, the nominal absorbed dose distribution is given (right).

FIGURE 5

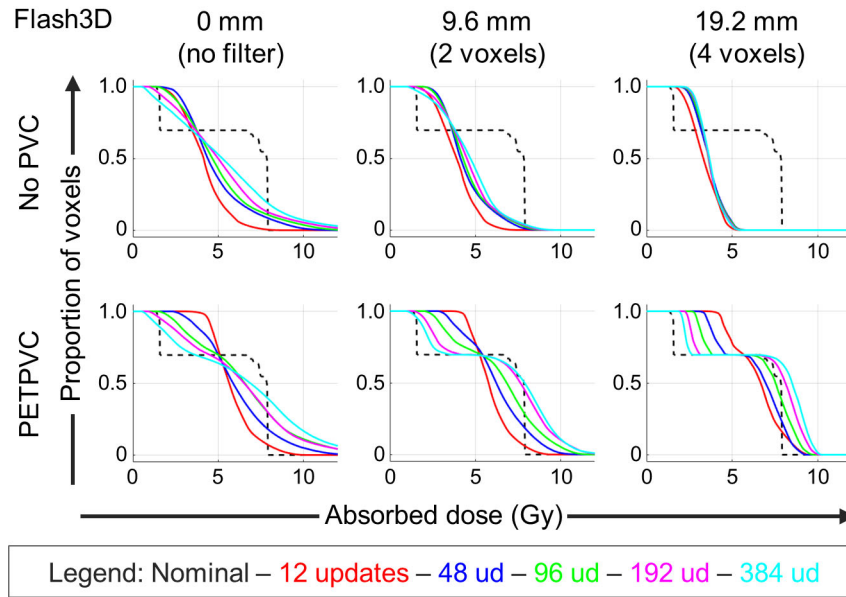


Figure 5. Cumulative dose volume histograms for different Flash3D reconstructions without (top) and with (bottom) partial-volume correction. From left to right, different post-filters are shown (no filtering, 2-voxel FWHM, 4-voxel FWHM). Additionally, different numbers of updates were applied (different colors). The nominal absorbed dose is given by the dashed black line.

FIGURE 6

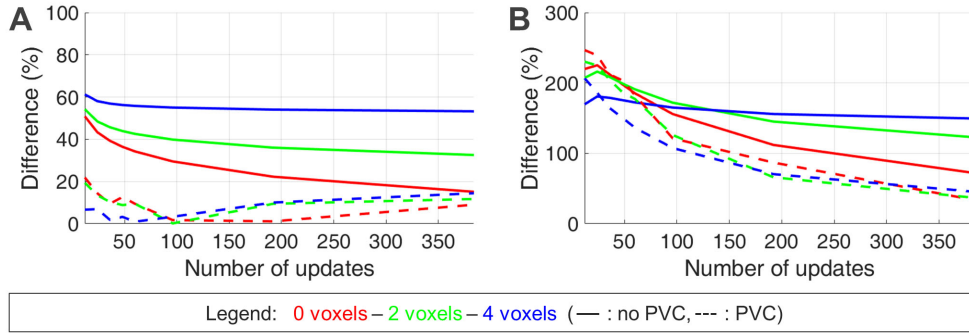


Figure 6. Percentage difference between the SPECT/CT-based and the HPGe-based mean sub-organ absorbed doses for different post-filters for Flash3D reconstructions with (dashed line) and without (solid line) partial-volume correction. A: Cortex. B: Medulla.

TABLE 1

Table 1: Predetermined resolutions for different combinations of iterations (abbreviation ‘12u’: 12 updates) and post-filters (‘FWHM’: Full width at half maximum of Gaussian post-filter). All numbers are given in millimeter.

	FWHM	12u	24u	36u	48u	96u	192u*	384u*	672u*	960u*
Flash3D	0 Voxels	13.4	11.5	10.8	8.8	9.3	6.9	6.5	5.3	5.7
	2 Voxels	16.1	14.1	13.3	12.6	12.5	11.9	11.5	10.9	11.1
	4 Voxels	25.6	21.8	21.9	20.7	20.7	21.0	21.0	21.2	21.2

*: The manufacturer restricts the number of iterations to 100. Therefore, 96 iterations were combined with 2 subsets (192 updates) and 4 subsets (384 updates) to achieve higher update numbers.

TABLE 2

Table 2: Mean sub-organ absorbed doses (cortex, medulla) and mean kidney organ absorbed dose in Gy for different numbers of updates (iterations * subsets) and post-filters (the FWHM is given as number of voxels). Reconstructions were performed with/without partial-volume correction (PETPVC). The best correlation to the nominal dose (top row) is marked in bold.

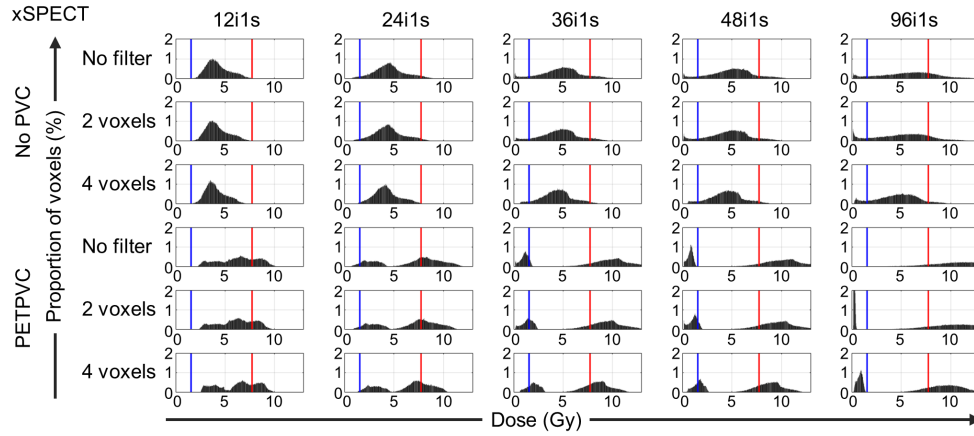
Compartment		Cortex		Medulla		Kidney	
Nominal		7.75		1.56		5.87	
	#Updates	No PVC	PETPVC	No PVC	PETPVC	No PVC	PETPVC
0 Voxels	12	3.81	6.05	5.00	5.42	4.17	5.86
	24	4.39	6.63	5.08	5.30	4.60	6.23
	36	4.70	7.01	4.87	4.87	4.76	6.36
	48	4.92	6.77	4.66	4.75	4.84	6.16
	60	5.09	7.02	4.46	4.42	4.90	6.23
	96	5.46	7.88	4.00	3.46	5.02	6.54
	192	6.02	7.83	3.31	2.92	5.20	6.34
	384	6.58	8.44	2.69	2.09	5.39	6.51
	672	6.94	8.44	2.23	1.76	5.51	6.41
	960	7.22	8.99	1.99	1.31	5.63	6.65
2 Voxels	12	3.55	6.25	4.80	5.16	3.93	5.92
	24	3.99	6.71	4.94	5.07	4.28	6.21
	36	4.21	6.95	4.82	4.75	4.39	6.28
	48	4.35	7.06	4.68	4.48	4.45	6.28
	60	4.45	7.01	4.55	4.33	4.48	6.20
	96	4.66	7.76	4.25	3.53	4.54	6.47
	192	4.96	8.48	3.83	2.59	4.61	6.69
	384	5.23	8.65	3.48	2.14	4.69	6.67
	672	5.38	8.67	3.23	1.88	4.73	6.60
	960	5.52	9.10	3.14	1.56	4.79	6.80
4 Voxels	12	3.00	7.23	4.21	4.79	3.37	6.49
	24	3.25	7.21	4.39	4.47	3.60	6.38
	36	3.34	7.61	4.36	4.13	3.65	6.55
	48	3.39	7.50	4.31	3.91	3.67	6.41
	60	3.42	7.67	4.26	3.69	3.68	6.46
	96	3.48	8.00	4.14	3.24	3.68	6.56
	192	3.56	8.52	4.00	2.66	3.69	6.74
	384	3.62	8.87	3.90	2.27	3.71	6.86
	672	3.64	9.08	3.82	2.01	3.69	6.93
	960	3.68	9.20	3.82	1.95	3.73	7.00

TABLE 3

Table 3: RMSD between the SPECT/CT-based and the nominal absorbed dose distribution in Gy for different numbers of updates (iterations * subsets) and post-filters (the FWHM is given as number of voxels). Reconstructions were performed with/without partial-volume correction (PETPVC). The best correlation to the nominal dose (top row) is marked in bold.

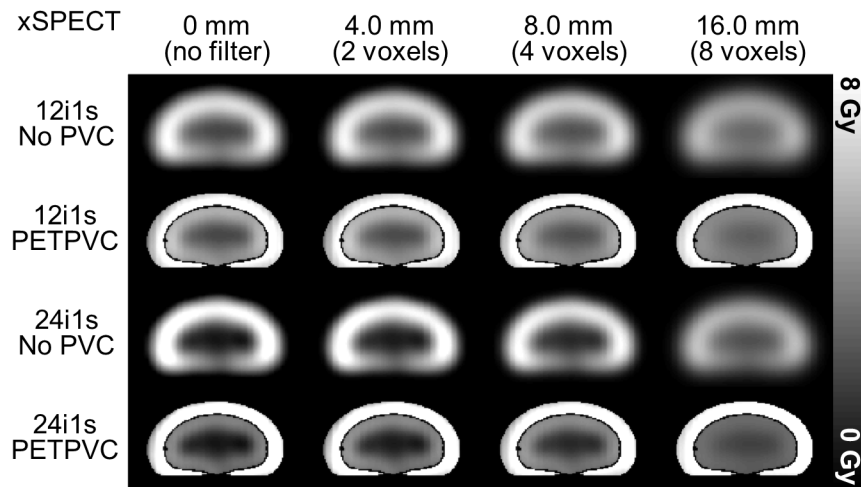
Compartment	#Updates	Cortex		Medulla		Kidney	
		No PVC	PETPVC	No PVC	PETPVC	No PVC	PETPVC
0 Voxels	12	4.11	2.06	3.56	3.97	3.95	2.78
	24	3.68	1.88	3.77	3.97	3.71	2.69
	36	3.49	1.89	3.67	3.60	3.54	2.53
	48	3.36	2.04	3.53	3.58	3.41	2.61
	60	3.26	2.03	3.40	3.27	3.30	2.47
	96	3.06	2.12	3.06	2.26	3.06	2.17
	192	2.83	2.29	2.55	1.89	2.75	2.17
	384	2.81	2.77	2.12	1.14	2.62	2.39
	672	3.01	3.14	1.86	1.07	2.71	2.69
	960	3.28	3.74	1.78	0.82	2.91	3.15
2 Voxels	12	4.30	1.80	3.32	3.67	4.03	2.52
	24	3.92	1.56	3.53	3.64	3.81	2.39
	36	3.74	1.48	3.47	3.34	3.66	2.22
	48	3.62	1.44	3.37	3.10	3.55	2.09
	60	3.53	1.44	3.28	2.97	3.46	2.03
	96	3.35	1.30	3.05	2.14	3.26	1.61
	192	3.07	1.50	2.73	1.19	2.98	1.41
	384	2.84	1.59	2.48	0.77	2.73	1.39
	672	2.71	1.63	2.30	0.58	2.59	1.40
	960	2.61	2.00	2.25	0.39	2.50	1.68
4 Voxels	12	4.79	0.97	2.70	3.26	4.26	1.97
	24	4.55	0.94	2.87	2.93	4.11	1.80
	36	4.46	0.82	2.85	2.59	4.04	1.59
	48	4.41	0.79	2.80	2.38	3.99	1.47
	60	4.37	0.73	2.76	2.16	3.95	1.34
	96	4.31	0.72	2.66	1.70	3.88	1.11
	192	4.23	0.98	2.52	1.12	3.80	1.02
	384	4.17	1.24	2.43	0.73	3.73	1.11
	672	4.15	1.44	2.35	0.47	3.70	1.23
	960	4.10	1.55	2.35	0.41	3.66	1.31

Supplemental Figure 1



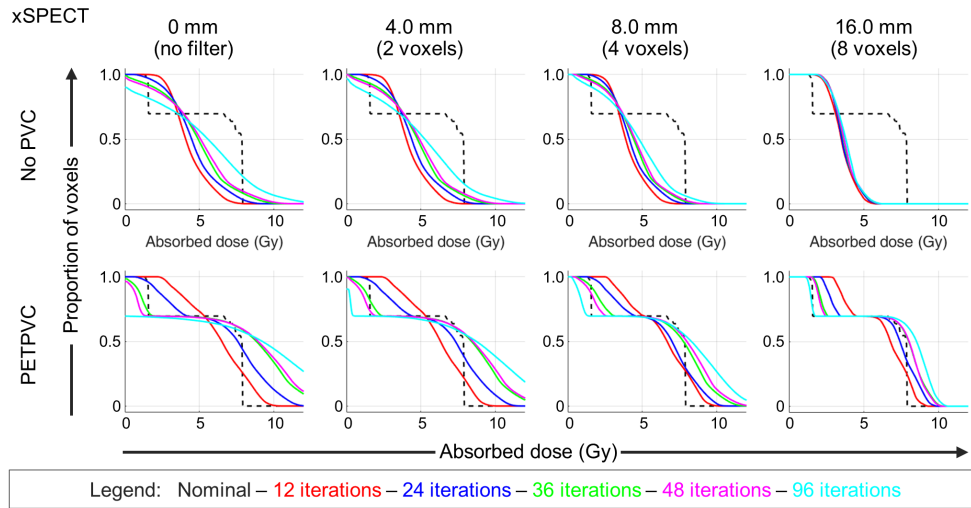
Differential dose volume histograms for different xSPECT Quant reconstructions without (top) and with (bottom) partial-volume correction. From left to right, different numbers of iterations are shown. Additionally, different post-filters were applied (no filtering, 2-voxel FWHM, 4-voxel FWHM). The blue and red solid lines indicate the nominal absorbed dose values of both compartments.

Supplemental Figure 2



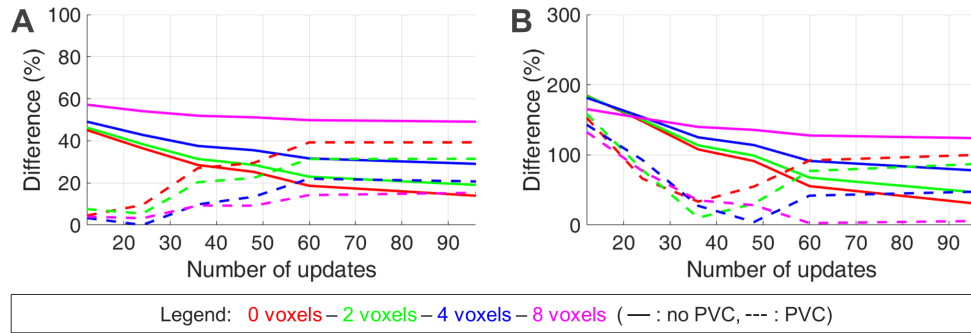
Cross-sections through the 3D absorbed dose distributions obtained from the xSPECT Quant reconstructions (12 and 24 updates) with and without partial-volume correction. From left to right, different post-filters were applied (no filtering, 2-voxel FWHM, 4-voxel FWHM, 8-voxel FWHM). Additionally, the nominal absorbed dose distribution is given (right).

Supplemental Figure 3



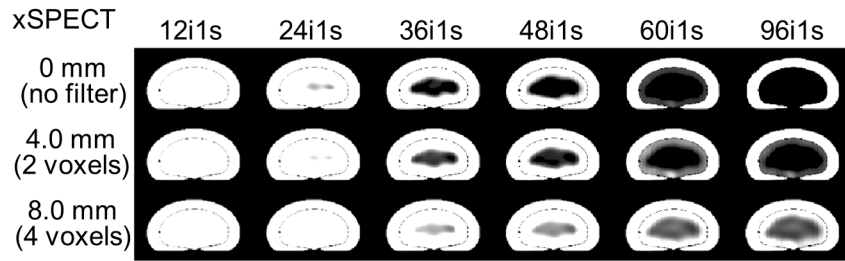
Cumulative dose volume histograms for different xSPECT Quant reconstructions without (top) and with (bottom) partial-volume correction. From left to right, different post-filters are shown (no filtering, 2-voxel FWHM, 4-voxel FWHM, 8-voxel FWHM). Additionally, different numbers of updates were applied (different colors). The nominal absorbed dose is given by the dashed black line.

Supplemental Figure 4



Percentage difference between the SPECT/CT-based and the HPGe-based mean sub-organ absorbed doses for different post-filters for xSPECT Quant reconstructions with (dashed line) and without (solid line) partial-volume correction. A: Cortex. B: Medulla.

Supplemental Figure 5



Cross-sections through the 3D absorbed dose distributions obtained from the xSPECT Quant reconstructions for different iteration numbers (left to right) without partial-volume correction. From top to bottom, different post-filters were applied (no filtering, 2-voxel FWHM, 4-voxel FWHM).